Journal of
Synchrotron
Radiation

ISSN 1600-5775

Received 25 June 2013
Accepted 30 September 2013

A facile heating cell for *in situ* transmittance and fluorescence X-ray absorption spectroscopy investigations

Pengfei An, Caihao Hong,* Jing Zhang, Wei Xu and Tiandou Hu

Beijing Synchrotron Radiation Facility, Institute of High Energy Physics, Chinese Academy of Sciences, Beijing 100049, People's Republic of China. *E-mail: hongch@ihep.ac.cn

A facile heating cell has been designed for *in situ* transmittance and fluorescence X-ray absorption spectroscopy (XAS) measurements up to 1273 K under vacuum or an inert atmosphere. These high temperatures are achieved using a tantalum heating element by ohmic heating. Because of the small specific heat capacity, the temperature can be changed in a matter of minutes from room temperature to high temperature. Furthermore, a commercial power controller was adapted to provide stable temperature control. The construction of the heat shielding system provides a novel approach to reducing the beam's path length and the cell's size. The cell is inexpensive and easy to build. Its performance was evaluated by *in situ* XAS measurements of the temperature-dependent structure of ceria nanocrystals. Some preliminary results for the structural mechanism in ceria nanocrystal redox applications are given.

Keywords: heating cell; *in situ*; transmittance and fluorescence; X-ray absorption spectroscopy.

© 2014 International Union of Crystallography

1. Introduction

The design, synthesis and manufacture of new materials with optimized functionalities require a sufficiently good understanding of the microstructure in the materials. X-ray absorption spectroscopy (XAS) is a powerful method for local geometric and electronic characterization in crystalline compounds, amorphous substances, glasses and liquids (Koningsberger & Prins, 1987). In many cases, structural information can be collected *in situ*, *i.e.* under well known temperature and atmospheric conditions. *In situ* high-temperature XAS measurements are of fundamental interest for a detailed understanding of temperature-dependent structures in phase-change materials (Kolobov *et al.*, 2004; Waychunas *et al.*, 1988). This method can also be used, for instance, to trace the growth of nanocrystals and redox reaction dynamics induced by temperature changes (Chen *et al.*, 2008; Kong *et al.*, 2012; Nashner *et al.*, 1998) and to reveal the relationship between a catalyst's structure and its reactivity (Frenkel *et al.*, 2012; Newton *et al.*, 2007; Yamamoto *et al.*, 2007).

To accomplish these tasks, several design approaches have been reported for versatile XAS cells (Bare *et al.*, 2006; Farges *et al.*, 1995; Girardon *et al.*, 2005; Guilera *et al.*, 2009; Huwe & Fröba, 2004; Longo *et al.*, 2005; Meitzner *et al.*, 1998). For example, Farges *et al.* (1995) applied the Mysen–Frantz heating-wire technique to design an XAS high-temperature cell for the study of metal oxide phase transitions. Girardon *et al.* (2005) proposed an XAS cell dedicated to *in situ* and *operando* experiments in heterogeneous catalysis. The cell can be used at ambient or elevated temperatures under the flow of a large variety of oxidizing or reducing gas mixtures. Huwe & Fröba (2004) designed and tested a high-temperature cell for *in situ* transmission and fluorescence XAS investigations. Furthermore, Guilera *et al.* (2009) built a miniature maxthal furnace for XAS experiments up to 1273 K.

Despite these recent advances, it is still a great challenge to design a high-quality cell that utilizes an inexpensive heater, convenient windows, a stable temperature controller and a compact volume. Here, we present a facile heating cell for *in situ* transmission and fluorescence XAS measurements up to 1273 K in a vacuum or an inert atmosphere. The high temperature is achieved by ohmic heating. Because of its high melting point and chemical stability, a tantalum heating element can also serve as a sample holder. The temperature can be changed in a matter of minutes from room temperature to high temperature and back because of the small heat capacity. The cell uses a commercial power controller and a silicon-controlled rectifier (SCR) voltage regulator module, so the temperature control precision of the system is $\pm 1‰$ over the range from room temperature to 1273 K. More importantly, a special X-ray window is stacked with kapton and carbon foils to form a heat shield system; this system provides a novel approach to reducing the beam's path length and to making the cell more compact. The cell is inexpensive and easy to build. Combined with quick-scanning XAS (QXAS)

Table 1
Important cell parameters.

Dimensions (length × width × height)	70 × 70 × 120 mm
Sample–window distance	35 mm
Temperature range	Room temperature to 1273 K
Heating power (at 1273 K)	75 W
Heating resistance (at 1273 K)	0.31 Ω
Heating electric current (at 1273 K)	56 A
Thermocouple	Chromel/alumel

techniques (Frahm, 1989; Prestipino *et al.*, 2011; Frenkel *et al.*, 2012), it is suitable for performing *in situ* investigations as demanded, *e.g.* metallic melts (Lou *et al.*, 2013), nanoparticles phase-change, and the solidification process of crystalline materials. Here, the cell's performance was evaluated by *in situ* XAS measurements of the temperature-dependent structure of ceria nanocrystals. The initial results for the structural mechanism in ceria nanocrystal redox applications are given.

2. *In situ* cell

The *in situ* X-ray absorption cell is displayed in Fig. 1. The cell consists of three main parts: (i) an aluminium chamber, which accommodates (ii) the heater and the sample holder system, and (iii) the temperature control system. The aluminium chamber is equipped with three windows to accommodate the incoming, transmitted and fluorescence X-rays. Special films made of stacks of kapton foil with a 10 µm thickness and graphite paper with a 100 µm thickness were fixed on each window with an O-ring. The black graphite paper can absorb thermal radiation from the heat element and prevents the direct exposure of the kapton foil to strong thermal radiation that would otherwise cause aging and cracking of the kapton foil. Fig. S1 of the supporting information[1] shows the effect of the carbon heat shield layer on the heating cell. When the cell is at high temperature without the heat shield, thermal radiation can be visually observed, and this radiation would eventually destroy the cell window. In addition, such a window is almost transparent to hard X-rays because its composition is mostly the light elements carbon, hydrogen and oxygen. Using this window, the beam's path length can be reduced, and the cell is more compact. The top/inner part of the cell is the heart of the cell. As shown in Fig. 2, the heater and sample holder can be removed to enable sample loading. The cell consists of current feedthroughs, a stainless steel fixture, a molybdenum fixture with a channel, and a tantalum-sheet heating element. Important cell parameters are listed in Table 1.

As depicted in Fig. 2, the heating element is made up of two pieces of 100 µm-thick tantalum sheets. The two tantalum sheets are welded together to create a pocket to mount the test sample. The size of the tantalum elements is 12 mm × 42 mm. An elongated hole is reserved in the middle of the tantalum sample pocket to allow the incident and outgoing X-rays to pass through. Such a pure metal heater has a small electrical resistivity. Therefore, a large current is needed to heat the

[1] Supporting information for this paper is available from the IUCr electronic archives (Reference: HF5239).

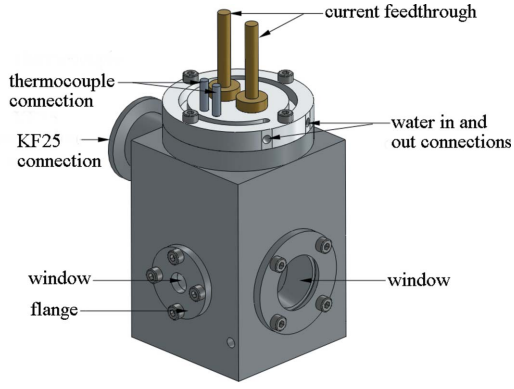

Figure 1
Structure and appearance of the *in situ* cell.

sample to high temperature. Two copper poles, 10 mm in diameter, are used as current feedthroughs. To minimize heat outflow from the copper poles, a molybdenum column and stainless steel bracket are used to decrease the thermoconductivity. They connect the copper poles to the tantalum heat element as show in Fig. 2. An additional tantalum sheet with a 0.1 mm thickness is present on the top of the sample holder, which further shields the thermal radiation from the heating system and localizes the heat intended to warm the test sample. A K-type thermocouple, 0.1 mm in diameter, is welded to the tantalum heater to monitor the temperature in the heating zone.

Because of the small heat capacity of the tantalum heater element, the temperature could be raised from room

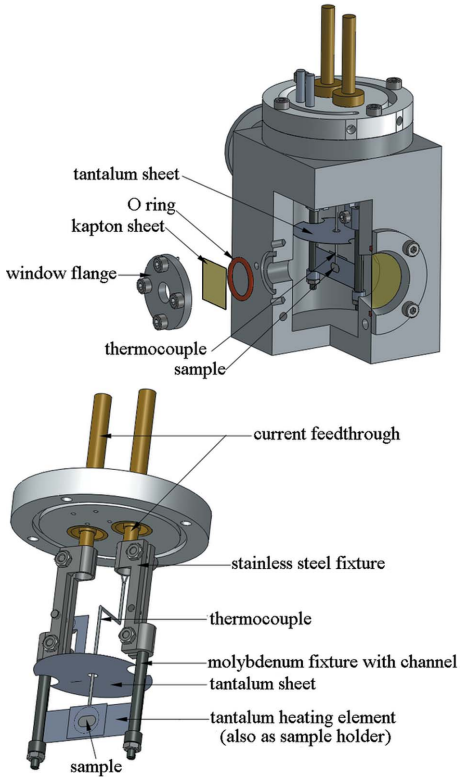

Figure 2
Top/inner part of the cell.

temperature to 1273 K in less than one minute and could drop back to room temperature in ten minutes. On the other hand, the heater element has a small resistance, so a large current is needed to drive it to reach high temperatures. To achieve system accuracy and stability, an optimized heating control system was introduced. This control system is made of a proportional-integral-differential (PID) controller (AIJ 908, Xiameng Yudian Automation Technology), a silicon-controlled rectifier (SCR) voltage regulator module (SSR-V2240A, Hangzhou Guojing Deji) and a transformer (220 VAC to 3 VAC). As shown in Fig. S2, the PID controller automatically adjusts the output power using the SCR voltage regulator according to the measured temperature. Fig. 3 shows the temperature curves when the cell is operated at the possible heating speeds under actual experiment conditions. The controlled temperature precision of the system is 1‰ over the range from room temperature to 1273 K, suggesting the temperature control system has the ability to heat the cell stably under actual experiment conditions.

As shown in Fig. 2, the thermocouple is used to monitor the temperature in the heating zone. However, the sample center temperature should always be lower than that of the monitor spot, due to a lacking tantalum heat element covering in the sample center. In order to calibrate the temperature difference between the center of the sample and the monitor spot on the tantalum heater, two thermocouples were used in the calibration experiment. One thermocouple was welded to the tantalum heater to monitor the temperature in the heating zone. The other was inserted into the center of a boron nitride pellet of 1 mm thickness and 10 mm diameter to show the actual temperature of the sample. At each set temperature point the temperatures of the thermocouples were recorded at the same time, as shown in Fig. 4. The value of the temperature difference R is lower than 1% from room temperature to 1000 K, and is lower than 4% when the temperature is between 1000 K and 1273 K, since the thermal radiation diffusing from the hot sample enlarges the temperature difference in the higher temperature range.

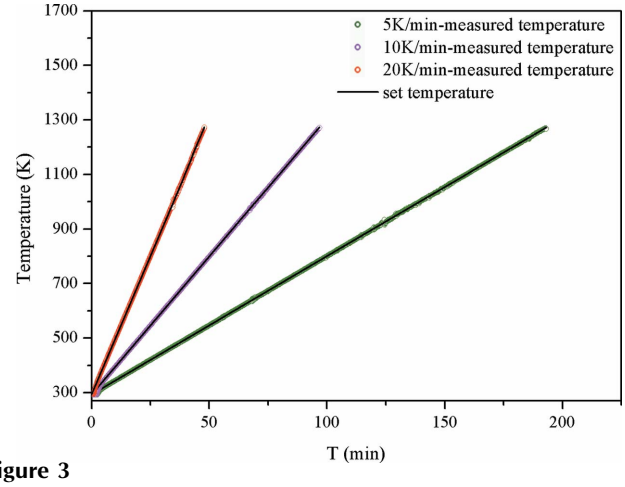

Figure 3
Temperature curves recorded under actual experiment conditions (*i.e.* at the sample position, under vacuum, with water cooling and an aligned sample holder).

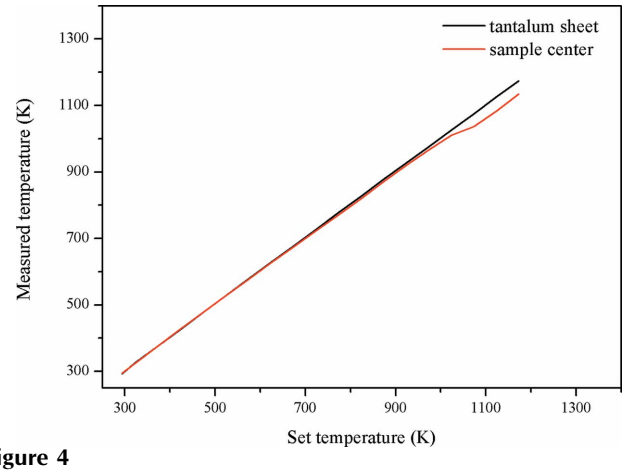

Figure 4
Temperature difference between the sample center and monitor spot on the tantalum heater.

Further, to avoid fast oxidation of the tantalum heating element in air, the heating cell can only be used under vacuum or an inert atmosphere. Vacuum was achieved using a rotary mechanical pump, and the operation pressure is several Pascals. The life time of the tantalum heating element is several hundred hours.

3. XAS measurements

The *in situ* cell was tested on the 1W1B beamline of the Beijing Synchrotron Radiation Facility, which was operating at 250 mA of stored current. For the *in situ* high-temperature measurements, ceria samples were pressed into a boron nitride pellet with a diameter of 10 mm and a thickness of ∼0.5–1 mm. The heating speed was 5 K min^{-1}. The XAS spectra were scanned in the range 5.5–6.2 keV, which covers the L_3-edge absorption of cerium atoms. Figs. 5(*a*) and 5(*b*) show the Ce L_3-edge XANES spectra of the ceria in nanocrystal form and in bulk. Based on the literature (Douillard *et al.*, 1995; Kaindl *et al.*, 1988; Modeshia *et al.*, 2007; Soldatov *et al.*, 1994), the standard CeO_2 XANES spectrum from 5710 to 5750 eV contains four peaks (labeled *A*, *B*, *C* and *D*). The pre-edge structure, labeled *D*, is assigned to final states with delocalized *d*-character at the bottom of the conduction band. Due to the cubic crystal-field splitting of Ce 5*d* states, features *B* and *C* are associated with the transitions of Ce 2*p* to the Ce $4f^15d_{eg}L$ and Ce $4f^15d_{t2g}L$ states, where *L* denotes an oxygen ligand 2*p* hole and $4f^1$ refers to an electron going from an oxygen 2*p* orbital to a cerium 4*f* orbital (charge-transfer-like transition). The energy separation between peaks *B* and *C* is approximately 3.6 eV, in agreement with previous works (Soldatov *et al.*, 1994). Feature *A* is attributed to the contribution of a different final state configuration, $4f^05d$. Generally, the Ce spectrum has a distinct double-peaked structure (*A* and *B*) with the higher lying peak corresponding to the Ce^{4+} valence state (Kaindl *et al.*, 1988; Soldatov *et al.*, 1994). As shown in Fig. 5(*c*), a significant change is observed in the ceria nanocrystals after an increase of the temperature. When the temperature rises to 1273 K, feature *A* disappears and a single

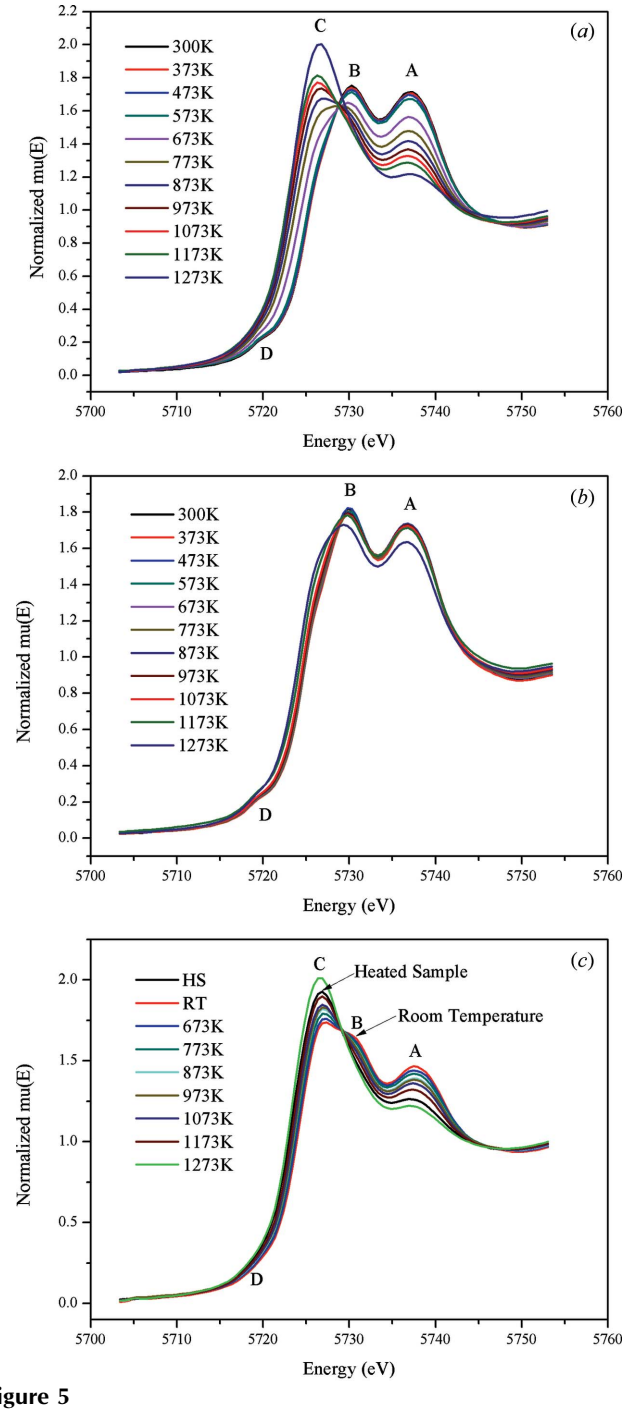

Figure 5
Effect of temperature on the Ce L_3-edge XANES spectra of ceria. (*a*) Nanoceria. (*b*) Bulk ceria. (*c*) Valence reversibility in nanoceria.

peak appears near *C*, which is shifted to a lower energy than *B* and suggests a change in the cerium oxidation state from +4 to +3 (Douillard *et al.*, 1995; Modeshia *et al.*, 2007). More interestingly, the spectroscopic valence changed back to +4 after the heated sample was kept under normal room conditions for several days. Additionally, the structural transformation is reversible when the sample is heated again. This reversibility is important because it provides a structural mechanism for the storage and release of oxygen that takes place in ceria in redox applications.

4. Conclusions

A facile heating cell was designed, constructed and applied. The cell can reach temperatures up to 1273 K and can record X-ray absorption spectra in transmission and fluorescence modes. The heat shielding system provides a novel approach to reducing the beam's path length and the cell size. Because of the small heat capacity of the tantalum heater element, the temperature of this system could be raised from room temperature to 1273 K in less than one minute and could drop back to room temperature in ten minutes. Using an optimized heating control system, the heater temperature precision was $\pm 1‰$ over the range from room temperature to 1273 K. The cell was successfully used to analyze the structural evolution of oxygen storage and release in ceria nanocrystals. Further, combined with QXAS techniques, the heating cell is very suitable for investigation of the temperature-dependent structure transition as demanded, *e.g.* metallic melts, nanoparticles phase-change and the solidification process of crystalline materials.

This work was financially supported by the National Natural Science Foundation of China (NSFC) (grant Nos. 11135008 and 11375229).

References

Bare, S. R., Mickelson, G. E., Modica, F. S., Ringwelski, A. Z. & Yang, N. (2006). *Rev. Sci. Instrum.* **77**, 023105.
Chen, X., Cai, Q., Wang, W., Mo, G., Jiang, L. S., Zhang, K. H., Chen, Z. J., Wu, Z. Y. & Wu, Z. H. (2008). *Chem. Mater.* **20**, 2757–2762.
Douillard, L., Gautier, M., Thromat, N. & Duraud, J. P. (1995). *Nucl. Instrum. Methods Phys. Res. B*, **97**, 133–136.
Farges, F., Itié, J.-P., Fiquet, G. & Andrault, D. (1995). *Nucl. Instrum. Methods Phys. Res. B*, **101**, 493–498.
Frahm, R. (1989). *Rev. Sci. Instrum.* **60**, 2515.
Frenkel, A. I., Rodriguez, J. A. & Chen, J. G. (2012). *ACS Catal.* **2**, 2269–2280.
Girardon, J.-S., Khodakov, A. Y., Capron, M., Cristol, S., Dujardin, C., Dhainaut, F., Nikitenko, S., Meneau, F., Bras, W. & Payen, E. (2005). *J. Synchrotron Rad.* **12**, 680–684.
Guilera, G., Gorges, B., Pascarelli, S., Vitoux, H., Newton, M. A., Prestipino, C., Nagai, Y. & Hara, N. (2009). *J. Synchrotron Rad.* **16**, 628–634.
Huwe, H. & Fröba, M. (2004). *J. Synchrotron Rad.* **11**, 363–365.
Kaindl, G., Schmiester, G., Sampathkumaran, E. & Wachter, P. (1988). *Phys. Rev. B*, **38**, 10174–10177.
Kolobov, A. V., Fons, P., Frenkel, A. I., Ankudinov, A. L., Tominaga, J. & Uruga, T. (2004). *Nat. Mater.* **3**, 703–708.
Kong, Q., Baudelet, F., Han, J., Chagnot, S., Barthe, L., Headspith, J., Goldsbrough, R., Picca, F. E. & Spalla, O. (2012). *Sci. Rep.* **2**, 1018.
Koningsberger, D. C. & Prins, R. (1987). *X-ray Absorption: Principles, Applications, Techniques of EXAFS, SEXAFS and XANES.* New York: John Wiley and Sons.
Longo, A., Balerna, A., d'Acapito, F., D'Anca, F., Giannici, F., Liotta, L. F., Pantaleo, G. & Martorana, A. (2005). *J. Synchrotron Rad.* **12**, 499–505.
Lou, H. B., Wang, X. D., Cao, Q. P., Zhang, D. X., Zhang, J., Hu, T. D., Mao, H.-K. & Jiang, J. Z. (2013). *Proc. Natl Acad. Sci.* **110**, 10068–10072.
Meitzner, G., Bare, S. R., Parker, D., Woo, H. & Fischer, D. A. (1998). *Rev. Sci. Instrum.* **69**, 2618.
Modeshia, D. R., Wright, C. S., Payne, J. L., Sankar, G., Fiddy, S. G. & Walton, R. I. (2007). *J. Phys. Chem. C*, **111**, 14035–14039.

Nashner, M. S., Frenkel, A. I., Somerville, D., Hills, C. W., Shapley, J. R. & Nuzzo, R. G. (1998). *J. Am. Chem. Soc.* **120**, 8093–8101.
Newton, M. A., Belver-Coldeira, C., Martínez-Arias, A. & Fernández-García, M. (2007). *Nat. Mater.* **6**, 528–532.
Prestipino, C., Mathon, O., Hino, R., Beteva, A. & Pascarelli, S. (2011). *J. Synchrotron Rad.* **18**, 176–182.
Soldatov, A., Ivanchenko, T., Della Longa, S., Kotani, A., Iwamoto, Y. & Bianconi, A. (1994). *Phys. Rev. B*, **50**, 5074–5080.
Waychunas, G. A., Brown, G. E. & Jackson, W. E. (1988). *Nature (London)*, **332**, 251–253.
Yamamoto, T., Suzuki, A., Nagai, Y., Tanabe, T., Dong, F., Inada, Y., Nomura, M., Tada, M., Iwasawa, Y. & Iwasawa, Y. (2007). *Angew. Chem.* **119**, 9413–9416.